# High-order eigenstate calculation of arbitrary quantum structures



2009 J. Phys. A: Math. Theor. 42 235201

(http://iopscience.iop.org/1751-8121/42/23/235201)

IOP PUBLISHING JOURNAL OF PHYSICS A: MATHEMATICAL AND THEORETICAL

J. Phys. A: Math. Theor. **42** (2009) 235201 (16pp) doi:10.1088/1751-8113/42/23/235201

# High-order eigenstate calculation of arbitrary quantum structures

**Daniel J Costinett**[1] **and Theodoros P Horikis**[2,3]

[1] Department of Electrical and Computer Engineering, 425 UCB, Boulder, CO 80309-0425, USA
[2] Department of Computer Science and Technology, University of Peloponnese, Tripolis 22100, Greece

E-mail: daniel.costinett@colorado.edu and horikis@uop.gr

Received 17 March 2009
Published 15 May 2009
Online at stacks.iop.org/JPhysA/42/235201

**Abstract**
Quantum engineering of electronic energy states using nanoscale layers of semiconductor compounds allows the design and the observation of quantum phenomena which are typically observed in atomic structures. Furthermore, semiconductors are present in nearly all modern electronic devices and are a crucial component of integrated circuits. Due to the relatively high rate of manufacturing defects, it is crucial to have a method for testing new semiconductor formations without requiring a sample to be fabricated. A simple, fast and very accurate numerical technique is presented to calculate the eigenstates of such arbitrary quantum structures. The method is based on a high-order finite difference scheme which allows the use of sparse matrix algebra, thus, significantly reducing computational time and allowing for high precision results even for the high energy states.

PACS numbers: 02.70.Bf, 03.65.Ge, 81.07.Bc

(Some figures in this article are in colour only in the electronic version)

## 1. Introduction

The Schrödinger equation plays a fundamental role in physics and in particular in quantum mechanics. It describes the quantum states of a physical system and as such it is as central to quantum mechanics as Newton's laws are to classical mechanics. In its time-independent form, the equation is a second-order, linear eigenvalue problem which until today has not been solved exactly for many physical systems. Even when an analytic solution is available, the resulting algebraic equations for the eigenvalues often involve complicated functions (ranging

[3] Author to whom any correspondence should be addressed.

  

from trigonometric to Airy) whose roots must be calculated numerically, thus making the use of numerical techniques unavoidable.

Important modern applications are based on this equation. For example, semiconductors are present in nearly all modern electronic devices and are a crucial component of integrated circuits. Because of their widespread use, it has become desirable to be able to create semiconductor material with highly specific conduction properties. For this purpose, many different materials are used in the fabrication of semiconductors. Additionally, the conduction properties of a material can be altered through doping, where impurities are introduced into a purified host material in a specific pattern. Doping can occur uniformly throughout an entire semiconductor to alter its overall properties, or in specific areas to define circuit elements within the material. The doping impurities may be dispersed as sparsely as 1 atom per $10^8$ atoms of substrate, requiring sophisticated instruments to accurately dope the material. Because of this, and the relatively high rate of manufacturing defects, it is crucial to have a method for testing new semiconductor formations without requiring a sample to be fabricated. The behavior of a doped semiconductor can be examined mathematically using the Schrödinger equation under the effective mass approximation [1] (see equation (1) below).

The most common approaches on the subject are finite element analysis [2, 3], the transfer matrix method [4, 5], variational [6] and shooting methods [7]. An iterative technique was presented in [8] and recently, a spectral grid method was introduced in [9]. A method for an interaction potential of general shape can be found in [10]. However, these methods need to be significantly modified if the potential profile changes, or need additional techniques to improve their accuracy. For example, none of the above cases consider asymmetric potentials or multiple potentials with all parameters of the problem discontinuous or singular across interfaces.

The first successful attempt to provide a method that takes into account all possible discontinuities was made in [11]. The basis of that method is the immersed interface method (IIM), first introduced in [12]. In its original formulation, the IIM is a second-order finite difference method that can be used to solve differential equations with discontinuous coefficients and singular sources. The main features of this method, that give it an immediate advantage over others, are that it requires no alternation for different types of potentials; the potential needs not be symmetric, it can be discontinuous and even singular in terms of delta functions. We give here its higher order generalization.

Our analysis is focused on the one-dimensional time-independent Schrödinger equation under the effective mass approximation, which in normalized form is given by

$$-\frac{1}{\pi^2}\frac{\mathrm{d}}{\mathrm{d}x}\left(\frac{1}{m^*}\frac{\mathrm{d}\psi}{\mathrm{d}x}\right)+V(x)\psi=\epsilon\psi \tag{1}$$

with normalized parameters $x = z/d, V = U/E_0, m^* = m_e/m_e(0), \epsilon = E/E_0$ and $E_0 = \hbar^2\pi^2/2m_e(0)d^2$, where $m_e(x)$ is the effective mass of the particle, $m_e(0)$ the effective mass of the particle at the origin, $d$ is the dimensional width of the well, $V(x)$ the potential and $E$ the energy of the particle. As usual $2\pi\hbar$ is Planck's constant. The potential $V(x)$ is an arbitrary function of $x$ and is bounded by semi-infinite flat barriers.

## 2. Formulation

To demonstrate the numerical scheme, we consider the Schrödinger equation in the form

$$-\frac{1}{\pi^2 m_*}\frac{\mathrm{d}^2\psi}{\mathrm{d}x^2}+V(x)\psi=\epsilon\psi,$$

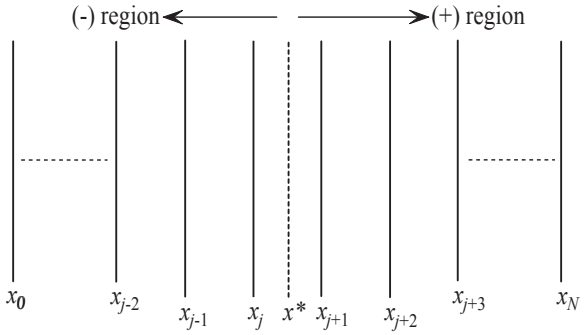


**Figure 1.** The uniform grid, the irregular points (longer solid lines) and the interface (longer dashed lines).

where all variables appear in nondimensional form and $-\infty < x < \infty$. Note that the choice of the equation causes no restriction in the implementation, efficiency or accuracy of the method; any linear, second-order equation can be treated in the same manner. To complete the boundary value problem we impose the boundary conditions $\psi(\pm\infty) = 0$ (see the appendix for further details on the boundary conditions). Furthermore, the mass of the particle is taken to be piecewise constant, hence, can be taken outside the derivative and any contributions from discontinuities will be incorporated in the numerical scheme below using appropriate matching conditions at the interfaces, where these discontinuities occur.

Define $M = M(x) = 1/\pi^2 m_*$ to further simplify the equation to

$$-M\psi_{xx} + V(x)\psi = \epsilon\psi, \tag{2}$$

where the subscripts denote differentiation. The function $M = M(x)$ is a piecewise constant and can be allowed to have a discontinuity at, say, $x = x^*$. For simplicity, and without loss of generality, we also assume that the potential $V(x)$ may also have a jump at $x = x^*$. The equation is numerically integrated over a uniform grid in the interval $[x_0, x_N]$ with $x_i = x_0 + hi$, $i = 0, 1, 2, \ldots, N-1$, where $h = (b-a)/(N-1)$. The point $x^*$ will naturally fall between two grid points, say $x_j \leqslant x^* < x_{j+1}$, as shown in figure 1. If the interface should happen to fall on a grid point that is taken to be $x^* = x_j$. The goal is to develop a finite difference approximation of the form

$$\sigma_1\psi_{i-2} + \sigma_2\psi_{i-1} + \sigma_3\psi_i + \sigma_4\psi_{i+1} + \sigma_5\psi_{i+2} = \epsilon\psi_i, \qquad i = 1, 2, \ldots, N-1 \tag{3}$$

that can be used together with the boundary conditions to obtain a fourth-order accurate approximation to $\psi(x)$. The points for which $i = j-1, j, j+1, j+2$, are called *irregular* since the differencing scheme, equation (3), is not satisfied (the interface is between two grid points, see figure 1). All other points are called *regular*. If the interface is not present the usual definition for $\sigma$'s apply, namely

$$\sigma_1 = \sigma_5 = \frac{M(x_i)}{12h^2}, \qquad \sigma_2 = \sigma_4 = \frac{-4M(x_i)}{3h^2}, \qquad \sigma_3 = \frac{5M(x_i)}{2h^2} + V(x_i)$$

which, also applies to all regular points. Essentially our goal is to determine the values of $\sigma$'s for all irregular points, so that fourth-order accuracy is maintained.

To do this we expand $\psi(x_i) = \psi_i$, $i = j-1, j, j+1, j+2$, in a Taylor series around the point $x = x^*$. Hereafter, the values of all function defined on the left of the interface (the (–) region) will be denoted with a – superscript, whereas the functions defined on the right (the

(+) region) will be denoted with a + superscript, namely $\psi^-$ and $\psi^+$. Then

$$\psi(x_{j-1}) = \psi_{j-1} = \psi^- + (x_{j-1} - x^*)\psi_x^- + \tfrac{1}{2}(x_{j-1} - x^*)^2\psi_{xx}^- + \tfrac{1}{6}(x_{j-1} - x^*)^3\psi_{xxx}^- + \tfrac{1}{24}(x_{j-1} - x^*)^4\psi_{xxxx}^-, \tag{4a}$$

$$\psi(x_j) = \psi_j = \psi^- + (x_j - x^*)\psi_x^- + \tfrac{1}{2}(x_j - x^*)^2\psi_{xx}^- + \tfrac{1}{6}(x_j - x^*)^3\psi_{xxx}^- + \tfrac{1}{24}(x_j - x^*)^4\psi_{xxxx}^-, \tag{4b}$$

$$\psi(x_{j+1}) = \psi_{j+1} = \psi^+ + (x_{j+1} - x^*)\psi_x^+ + \tfrac{1}{2}(x_{j+1} - x^*)^2\psi_{xx}^+ + \tfrac{1}{6}(x_{j+1} - x^*)^3\psi_{xxx}^+ + \tfrac{1}{24}(x_{j+1} - x^*)^4\psi_{xxxx}^+, \tag{4c}$$

$$\psi(x_{j+2}) = \psi_{j+2} = \psi^+ + (x_{j+2} - x^*)\psi_x^+ + \tfrac{1}{2}(x_{j+2} - x^*)^2\psi_{xx}^+ + \tfrac{1}{6}(x_{j+2} - x^*)^3\psi_{xxx}^+ + \tfrac{1}{24}(x_{j+2} - x^*)^4\psi_{xxxx}^+. \tag{4d}$$

The right-hand side of equation (3) is expanded as follows:

$$\begin{aligned}
\epsilon\psi_j &= \epsilon\left[\psi^- + (x_j - x^*)\psi_x^- + \frac{1}{2}(x_j - x^*)^2\psi_{xx}^-\right] \\
&= \left(-M^-\psi_{xx}^- + V^-\psi^-\right) + (x_j - x^*)\left(-M^-\psi_{xxx}^- + V_x^-\psi^- + V^-\psi_x^-\right) \\
&\quad + \frac{1}{2}(x_j - x^*)^2\left(-M^-\psi_{xxxx}^- + V_{xx}^-\psi^- + 2V_x^-\psi_x^- + V^-\psi_{xx}^-\right) \\
&= \psi^-\left[V^- + (x_j - x^*)V_x^- + \frac{1}{2}(x_j - x^*)^2V_{xx}^-\right] \\
&\quad + \psi_x^-\left[(x_j - x^*)V^- + (x_j - x^*)^2V_x^-\right] \\
&\quad + \psi_{xx}^-\left[-M^- + \frac{1}{2}(x_j - x^*)^2V^-\right] + \psi_{xxx}^-[-M^-(x_j - x^*)] \\
&\quad + \psi_{xxxx}\left[-\frac{M^-}{2}(x_j - x^*)^2\right],
\end{aligned} \tag{5}$$

where equation (2) and its first and second derivatives have been used. Next we substitute equations (2) and (5) into equation (3) and match relative terms of $\psi$ and its derivatives from both sides of the resulting equation. Note, however, that equations (4*c*) and (4*d*) involve the values of $\psi$ (and its derivatives) evaluated at the (+) region. We therefore need relations to connect the functions and their relative values in the two regions. These relations we call *jump conditions*. The first condition is the continuity of $\psi$, namely

$$\psi^+ = \psi^- = \psi.$$

The second comes from integrating equation (1) around the interface, namely

$$\lim_{\Delta x\to 0}\int_{x^*-\Delta x}^{x^*+\Delta x}\left(-\frac{1}{\pi^2}\frac{\mathrm{d}}{\mathrm{d}x}\left(\frac{1}{m^*}\frac{\mathrm{d}\psi}{\mathrm{d}x}\right) + V(x)\psi\right)\mathrm{d}x = \epsilon\lim_{\Delta x\to 0}\int_{x^*-\Delta x}^{x^*+\Delta x}\psi\,\mathrm{d}x.$$

Since $\psi$ is continuous across the interface the second relation becomes

$$\psi_x^+ = \frac{M^-}{M^+}\psi_x^-.$$

Using the above jump conditions and differentiating the equation twice we obtain the remaining jumps, on the second derivative ($\epsilon\psi^- = \epsilon\psi^+$)

$$\psi_{xx}^+ = \psi_{xx}^-\frac{M^-}{M^+} + \psi\frac{V^+ - V^-}{M^+}$$

the third derivative

$$\psi^+_{xxx} = \psi^-_{xxx}\left(\frac{M^-}{M^+}\right)^2 + \psi^-_x\left[\frac{M^-}{M^{+2}}(V^+ - V^-)\right] + \psi\left[\frac{V^+_x}{M^+} - \frac{M^-}{M^{+2}}V^-_x\right]$$

and the fourth derivative

$$\psi^+_{xxxx} = \psi^-_{xxxx}\left(\frac{M^-}{M^+}\right)^2 + \psi^-_{xx}\left[2\frac{M^-}{M^{+2}}(V^+ - V^-)\right] + \psi^-_x\left[2\frac{M^-}{M^{+2}}(V^+_x - V^-_x)\right]$$
$$+\psi\left[\frac{-M^-}{M^{+2}}V^-_{xx} + \frac{V^+_{xx}}{M^+} + \left(\frac{V^+ - V^-}{M^+}\right)^2\right].$$

Finally replacing these values and matching relevant terms we obtain for $\psi$

$$\begin{aligned}
&\sigma_1 + \sigma_2 + \sigma_3 + \sigma_4\left[1 + \frac{V^+ - V^-}{2M^+}(x_{j+1} - x^*)^2 + \frac{1}{6}\left(-\frac{M^-V^-_x}{M^{+2}} + \frac{V^+_x}{M^+}\right)(x_{j+1} - x^*)^3\right.\\
&\qquad\left. + \frac{1}{24}\left(\frac{(V^- - V^+)^2}{M^{+2}} - \frac{M^-}{M^{+2}}V^-_{xx} + \frac{1}{M^+}V^+_{xx}\right)(x_{j+1} - x^*)^4\right]\\
&\qquad +\sigma_5\left[1 + \frac{V^+ - V^-}{2M^+}(x_{j+2} - x^*)^2 + \frac{1}{6}\left(-\frac{M^-V^-_x}{M^{+2}} + \frac{V^+_x}{M^+}\right)(x_{j+2} - x^*)^3\right.\\
&\qquad\left. + \frac{1}{24}\left(\frac{(V^- - V^+)^2}{M^{+2}} - \frac{M^-}{M^{+2}}V^-_{xx} + \frac{1}{M^+}V^+_{xx}\right)(x_{j+2} - x^*)^4\right]\\
&\quad = V^- + (x_j - x^*)V^-_x + \frac{1}{2}(x_j - x^*)^2V^-_{xx}
\end{aligned}$$

for $\psi^-_x$

$$\begin{aligned}
&\sigma_1(x_{j-2} - x^*) + \sigma_2(x_{j-1} - x^*) + \sigma_3(x_j - x^*)\\
&\qquad +\sigma_4\left[(x_{j+1} - x^*)\frac{M^-}{M^+} + \frac{1}{6}(x_{j+1} - x^*)^3\frac{M^-}{M^{+2}}(V^+ - V^-)\right.\\
&\qquad\left. + \frac{1}{24}(x_{j+1} - x^*)^4\frac{M^-}{M^{+2}}2\left(V^+_x - V^-_x\right)\right]\\
&\qquad +\sigma_5\left[(x_{j+2} - x^*)\frac{M^-}{M^+} + \frac{1}{6}(x_{j+2} - x^*)^3\frac{M^-}{M^{+2}}(V^+ - V^-)\right.\\
&\qquad\left. + \frac{1}{24}(x_{j+2} - x^*)^4\frac{M^-}{M^{+2}}2\left(V^+_x - V^-_x\right)\right] = (x_j - x^*)V^- + (x_j - x^*)^2V^-_x
\end{aligned}$$

for $\psi^-_{xx}$

$$\begin{aligned}
&\sigma_1\frac{1}{2}(x_{j-2} - x^*)^2 + \sigma_2\frac{1}{2}(x_{j-1} - x^*)^2 + \sigma_3\frac{1}{2}(x_j - x^*)^2\\
&\qquad +\sigma_4\left[\frac{1}{2}(x_{j+1} - x^*)^2\frac{M^-}{M^+} + \frac{1}{24}(x_{j+1} - x^*)^4\frac{M^-}{M^{+2}}2(V^+ - V^-)\right]\\
&\qquad +\sigma_5\left[\frac{1}{2}(x_{j+2} - x^*)^2\frac{M^-}{M^+} + \frac{1}{24}(x_{j+2} - x^*)^4\frac{M^-}{M^{+2}}2(V^+ - V^-)\right]\\
&\quad = -M^- + \frac{1}{2}(x_j - x^*)^2V^-
\end{aligned}$$

for $\psi^-_{xxx}$

$$\sigma_1\frac{1}{6}(x_{j-2}-x^*)^3+\sigma_2\frac{1}{6}(x_{j-1}-x^*)^3+\sigma_3\frac{1}{6}(x_j-x^*)^3+\sigma_4\left[\frac{1}{6}(x_{j+1}-x^*)^3\left(\frac{M^-}{M^+}\right)^2\right]$$
$$+\sigma_5\left[\frac{1}{6}(x_{j+2}-x^*)^3\left(\frac{M^-}{M^+}\right)^2\right]=-M^-(x_j-x^*)$$

and for $\psi^-_{xxxx}$

$$\sigma_1\frac{1}{24}(x_{j-2}-x^*)^4+\sigma_2\frac{1}{24}(x_{j-1}-x^*)^4+\sigma_3\frac{1}{24}(x_j-x^*)^4+\sigma_4\left[\frac{1}{24}(x_{j+1}-x^*)^4\left(\frac{M^-}{M^+}\right)^2\right]$$
$$+\sigma_5\left[\frac{1}{24}(x_{j+2}-x^*)^4\left(\frac{M^-}{M^+}\right)^2\right]=-\frac{M^-}{2}(x_j-x^*)^2.$$

The above equations form a $5\times5$ linear system with unknowns of finite difference coefficients $\sigma$'s. The solution of this system provides the appropriate fourth-order corrections for equation (3) at the point $x_j$.

In a similar manner we obtain the systems at $x_{j-1}$,

$$\sigma_1+\sigma_2+\sigma_3+\sigma_4+\sigma_5\left[1+\frac{V^+-V^-}{2M^+}(x_{j+1}-x^*)^2+\frac{1}{6}\left(-\frac{M^-V^-_x}{M^{+2}}+\frac{V^+_x}{M^+}\right)(x_{j+1}-x^*)^3\right.$$
$$\left.+\frac{1}{24}\left(\frac{(V^--V^+)^2}{M^{+2}}-\frac{M^-}{M^{+2}}V^-_{xx}+\frac{1}{M^+}V^+_{xx}\right)(x_{j+1}-x^*)^4\right]$$
$$=V^-+(x_{j-1}-x^*)V^-_x+\frac{1}{2}(x_{j-1}-x^*)^2V^-_{xx},$$
$$\sigma_1(x_{j-3}-x^*)+\sigma_2(x_{j-2}-x^*)+\sigma_3(x_{j-1}-x^*)+\sigma_4(x_j-x^*)$$
$$+\sigma_5\left[(x_{j+1}-x^*)\frac{M^-}{M^+}+\frac{1}{6}(x_{j+1}-x^*)^3\frac{M^-}{M^{+2}}(V^+-V^-)\right.$$
$$\left.+\frac{1}{24}(x_{j+1}-x^*)^4\frac{M^-}{M^{+2}}2(V^+_x-V^-_x)\right]=(x_{j-1}-x^*)V^-+(x_{j-1}-x^*)^2V^-_x,$$
$$\sigma_1\frac{1}{2}(x_{j-3}-x^*)^2+\sigma_2\frac{1}{2}(x_{j-2}-x^*)^2+\sigma_3\frac{1}{2}(x_{j-1}-x^*)^2+\sigma_4\frac{1}{2}(x_j-x^*)^2$$
$$+\sigma_5\left[\frac{1}{2}(x_{j+1}-x^*)^2\frac{M^-}{M^+}+\frac{1}{24}(x_{j+1}-x^*)^4\frac{M^-}{M^{+2}}2(V^+-V^-)\right]$$
$$=-M^-+\frac{1}{2}(x_{j-1}-x^*)^2V^-,$$
$$\sigma_1\frac{1}{6}(x_{j-3}-x^*)^3+\sigma_2\frac{1}{6}(x_{j-2}-x^*)^3+\sigma_3\frac{1}{6}(x_{j-1}-x^*)^3+\sigma_4\frac{1}{6}(x_j-x^*)^3$$
$$+\sigma_5\left[\frac{1}{6}(x_{j+1}-x^*)^3\left(\frac{M^-}{M^+}\right)^2\right]=-M^-(x_{j-1}-x^*),$$
$$\sigma_1\frac{1}{24}(x_{j-3}-x^*)^4+\sigma_2\frac{1}{24}(x_{j-2}-x^*)^4+\sigma_3\frac{1}{24}(x_{j-1}-x^*)^4+\sigma_4\frac{1}{24}(x_j-x^*)^4$$
$$+\sigma_5\left[\frac{1}{24}(x_{j+1}-x^*)^4\left(\frac{M^-}{M^+}\right)^2\right]=-\frac{M^-}{2}(x_{j-1}-x^*)^2$$

at $x_{j+1}$,

$$\sigma_1\left[1+\frac{V^- - V^+}{2M^-}(x_{j-1}-x^*)^2+\frac{1}{6}\left(-\frac{M^+V_x^+}{M^{-2}}+\frac{V_x^-}{M^-}\right)(x_{j-1}-x^*)^3\right.$$
$$\left.+\frac{1}{24}\left(\frac{(V^+-V^-)^2}{M^{-2}}-\frac{M^+}{M^{-2}}V_{xx}^+ +\frac{1}{M^-}V_{xx}^-\right)(x_{j-1}-x^*)^4\right]$$
$$+\sigma_2\left[1+\frac{V^- - V^+}{2M^-}(x_j-x^*)^2+\frac{1}{6}\left(-\frac{M^+V_x^+}{M^{-2}}+\frac{V_x^-}{M^-}\right)(x_j-x^*)^3\right]$$
$$+\frac{1}{24}\left(\frac{(V^+-V^-)^2}{M^{-2}}-\frac{M^+}{M^{-2}}V_{xx}^+ +\frac{1}{M^-}V_{xx}^-\right)(x_j-x^*)^4\Bigg]$$
$$+\sigma_3+\sigma_4+\sigma_5 = V^+ +(x_{j+1}-x^*)V_x^+ +\frac{1}{2}(x_{j+1}-x^*)^2V_{xx}^+,$$

$$\sigma_1\left[(x_{j-1}-x^*)\frac{M^+}{M^-}+\frac{1}{6}(x_{j-1}-x^*)^3\frac{M^+}{M^{-2}}(V^- - V^+)+\frac{1}{24}(x_{j-1}-x^*)^4\frac{M^+}{M^{-2}}2\left(V_x^- - V_x^+\right)\right]$$
$$+\sigma_2\left[(x_j-x^*)\frac{M^+}{M^-}+\frac{1}{6}(x_j-x^*)^3\frac{M^+}{M^{-2}}(V^- - V^+)\right.$$
$$\left.+\frac{1}{24}(x_j-x^*)^4\frac{M^+}{M^{-2}}2\left(V_x^- - V_x^+\right)\right]+\sigma_3(x_{j+1}-x^*)+\sigma_4(x_{j+2}-x^*)$$
$$+\sigma_5(x_{j+3}-x^*) = (x_{j+1}-x^*)V^+ +(x_{j+1}-x^*)^2V_x^+,$$

$$\sigma_1\left[\frac{1}{2}(x_{j-1}-x^*)^2\frac{M^+}{M^-}+\frac{1}{24}(x_{j-1}-x^*)^4\frac{M^+}{M^{-2}}2(V^- - V^+)\right]$$
$$+\sigma_2\left[\frac{1}{2}(x_j-x^*)^2\frac{M^+}{M^-}+\frac{1}{24}(x_j-x^*)^4\frac{M^+}{M^{-2}}2(V^- - V^+)\right]$$
$$+\sigma_3\frac{1}{2}(x_{j+1}-x^*)^2+\sigma_4\frac{1}{2}(x_{j+2}-x^*)^2+\sigma_5\frac{1}{2}(x_{j+3}-x^*)^2$$
$$= -M^+ +\frac{1}{2}(x_{j+1}-x^*)^2V^+,$$

$$\sigma_1\left[\frac{1}{6}(x_{j-1}-x^*)^3\left(\frac{M^+}{M^-}\right)^2\right]+\sigma_2\left[\frac{1}{6}(x_j-x^*)^3\left(\frac{M^+}{M^-}\right)^2\right]$$
$$+\sigma_3\frac{1}{6}(x_{j+1}-x^*)^3+\sigma_4\frac{1}{6}(x_{j+2}-x^*)^3+\sigma_5\frac{1}{6}(x_{j+3}-x^*)^3 = -M^+(x_{j+1}-x^*),$$

$$\sigma_1\left[\frac{1}{24}(x_{j-1}-x^*)^4\left(\frac{M^+}{M^-}\right)^2\right]+\sigma_2\left[\frac{1}{24}(x_j-x^*)^4\left(\frac{M^+}{M^-}\right)^2\right]+\sigma_3\frac{1}{24}(x_{j+1}-x^*)^4$$
$$+\sigma_4\frac{1}{24}(x_{j+2}-x^*)^4+\sigma_5\frac{1}{24}(x_{j+3}-x^*)^4 = -\frac{M^+}{2}(x_{j+1}-x^*)^2,$$

and $x_{j+2}$

$$\sigma_1\left[1+\frac{V^- - V^+}{2M^-}(x_j-x^*)^2+\frac{1}{6}\left(-\frac{M^+V_x^+}{M^{-2}}+\frac{V_x^-}{M^-}\right)(x_j-x^*)^3\right.$$
$$\left.+\frac{1}{24}\left(\frac{(V^+-V^-)^2}{M^{-2}}-\frac{M^+}{M^{-2}}V_{xx}^+ +\frac{1}{M^-}V_{xx}^-\right)(x_j-x^*)^4\right]$$
$$+\sigma_2+\sigma_3+\sigma_4+\sigma_5 = V^+ +(x_{j+2}-x^*)V_x^+ +\frac{1}{2}(x_{j+2}-x^*)^2V_{xx}^+,$$

$$\sigma_1\left[(x_j-x^*)\frac{M^+}{M^-}+\frac{1}{6}(x_j-x^*)^3\frac{M^+}{M^{-2}}(V^--V^+)+\frac{1}{24}(x_j-x^*)^4\frac{M^+}{M^{-2}}2\left(V_x^--V_x^+\right)\right]$$
$$+\sigma_2(x_{j+1}-x^*)+\sigma_3(x_{j+2}-x^*)+\sigma_4(x_{j+3}-x^*)+\sigma_5(x_{j+4}-x^*)$$
$$=(x_{j+2}-x^*)V^++(x_{j+2}-x^*)^2V_x^+,$$
$$\sigma_1\left[\frac{1}{2}(x_j-x^*)^2\frac{M^+}{M^-}+\frac{1}{24}(x_j-x^*)^4\frac{M^+}{M^{-2}}2(V^--V^+)\right]+\sigma_2\frac{1}{2}(x_{j+1}-x^*)^2+\sigma_3\frac{1}{2}(x_{j+2}-x^*)^2$$
$$+\sigma_4\frac{1}{2}(x_{j+3}-x^*)^2+\sigma_5\frac{1}{2}(x_{j+4}-x^*)^2=-M^++\frac{1}{2}(x_{j+2}-x^*)^2V^+,$$
$$\sigma_1\left[\frac{1}{6}(x_j-x^*)^3\left(\frac{M^+}{M^-}\right)^2\right]+\sigma_2\frac{1}{6}(x_{j+1}-x^*)^3+\sigma_3\frac{1}{6}(x_{j+2}-x^*)^3+\sigma_4\frac{1}{6}(x_{j+3}-x^*)^3$$
$$+\sigma_5\frac{1}{6}(x_{j+4}-x^*)^3=-M^+(x_{j+2}-x^*),$$
$$\sigma_1\left[\frac{1}{24}(x_j-x^*)^4\left(\frac{M^+}{M^-}\right)^2\right]+\sigma_2\frac{1}{24}(x_{j+1}-x^*)^4+\sigma_3\frac{1}{24}(x_{j+2}-x^*)^4+\sigma_4\frac{1}{24}(x_{j+3}-x^*)^4$$
$$+\sigma_5\frac{1}{24}(x_{j+4}-x^*)^4=-\frac{M^+}{2}(x_{j+2}-x^*)^2.$$

Note that for the last two systems, at $x_{j+1}$ and $x_{j+2}$ the values on the (–) region are substituted with appropriate jump conditions on the (+) region.

The solutions of the above systems complete the difference equation (3) for all points $x_i$ and any possible discontinuities at $x^*$ are now included in the finite difference coefficients. The systems are the same for all interfaces, with appropriate changes in the coefficients, for the location of $x^*$, allowing one to analyze multiple quantum wells without having to change the formalism. More importantly, discontinuities for all functions are allowed, the matrix remains sparse, and the resulting method remains $O(h^4)$. Note finally, that the general form of the potential is irrelevant for the above corrections. The discretization of the potential affects only the general form of the coefficients and only its values before and after $x^*$ contribute to the systems above. This is another aspect that makes the method so efficient and capable of handling truly arbitrary potential profiles.

In the following sections, we numerically solve equation (1) not only for a variety of physically important potentials, but for artificially constructed ones that demonstrate the efficiency of our method.

## 3. Single potentials

In most cases of single potentials in the literature, constant or truncated parabolic potentials have been considered. To demonstrate the accuracy and convergence of our method we turn to another potential, which still possesses an exact solution and is somehow less trivial to solve. The delta potential is a common theoretical problem of quantum mechanics. It consists of the time-independent Schrödinger equation for a particle in a potential well defined by a Dirac delta function in one dimension. The delta function potential well is a special case of the finite potential well, and follows as a limit as the depth goes to infinity and the width goes to zero, keeping their product constant. The exact solution is of the form $\exp(-|x|)$ which suggests a jump in its derivatives at $x=0$, making it the first test case for our method.

For simplicity take equation (1) in the form

$$\frac{\mathrm{d}^2\psi}{\mathrm{d}x^2}-2\delta(x)\psi=-2\epsilon\psi. \tag{6}$$

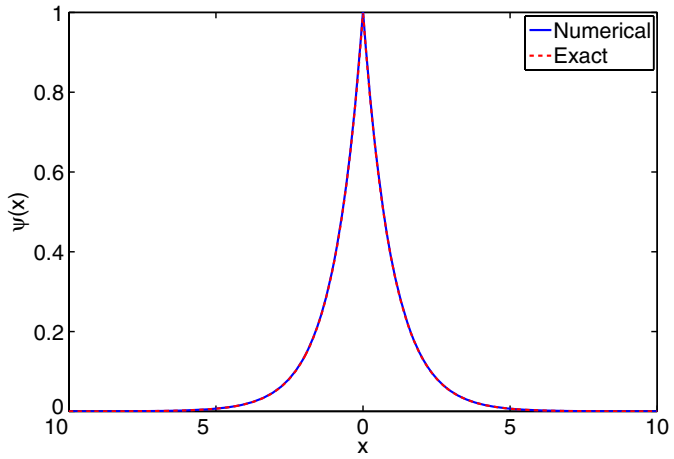


**Figure 2.** Exact and numerical solution of the Schrödinger equation for the delta potential.

**Table 1.** The energy for a delta potential with second and fourth-order accuracy.

| Number of points | Second-order results | Fourth-order results |
|---|---|---|
| 500 | −0.500 031 23 | −0.500 000 130 |
| 1 000 | −0.500 003 95 | −0.500 000 009 58 |
| 2 000 | −0.500 000 497 | −0.500 000 000 645 |
| 5 000 | −0.500 000 0319 | −0.500 000 000 0177 |
| 10 000 | −0.500 000 003 99 | −0.500 000 000 0000 |

The exact solution of the equation is $\psi(x) = A\exp(-|x|)$ and the corresponding eigenenergy is $\epsilon = -1/2$. To apply the above method one needs only to make a minor adjustment in the jump condition of the first derivative. Indeed, integrating equation (6) around $x = x^* = 0$ one gets $\psi_x^+ - \psi_x^- = 2\psi$, since as before $\psi^+ = \psi^- = \psi$. The remaining steps are used with no alterations. In figure 2 we plot the exact solution and the solution as obtained from our method, normalized so that $\psi(0) = 1$. In table 1 we show the convergence of the second and higher order methods. Note that the usual rule for significant digits is not followed for a reason: to demonstrate the accuracy and convergence of the two approaches. Every time we increase the number of points we show three additional digits. Results are clearly in excellent agreement with the expected value for the eigenenergy. The second-order method is summarized in the appendix.

Next we proceed to consider arbitrary shaped potentials. The first case is taken from [8] and concerns a linearly graded well with width 100 Å, height 0.48 eV and composition grading 0.2 eV. The first three energy states and the corresponding density functions are shown in figure 3. The well consists of $Al_{0.33}Ga_{0.67}As$ surrounded by GaAs barriers.

In in-well doped single quantum wells, ionized donors and free electrons exist together in the quantum well, so cancellation of the charges occurs. This charge screening effect suppresses band bending outside of the quantum well, even in high donor densities. As a result of the cancellation between the interactive force from ionized donors and the repulsive force among the free electrons themselves, the change in the distribution of the free electrons is fairly well suppressed. For more on the physical importance of these wells one can see [6]. Take

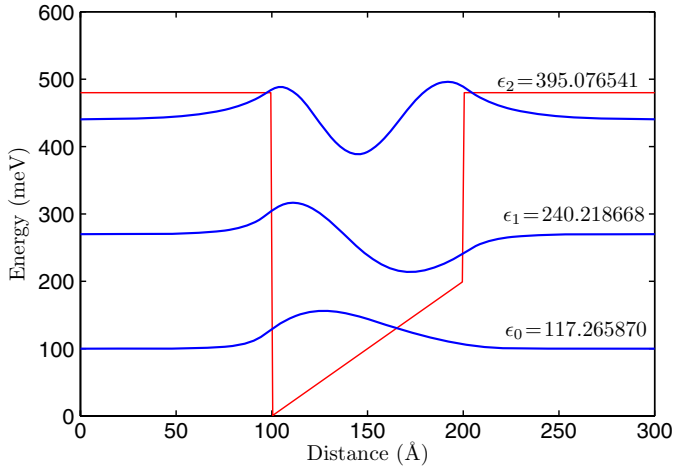


**Figure 3.** Eigenstates of the linearly graded quantum well described in the text.

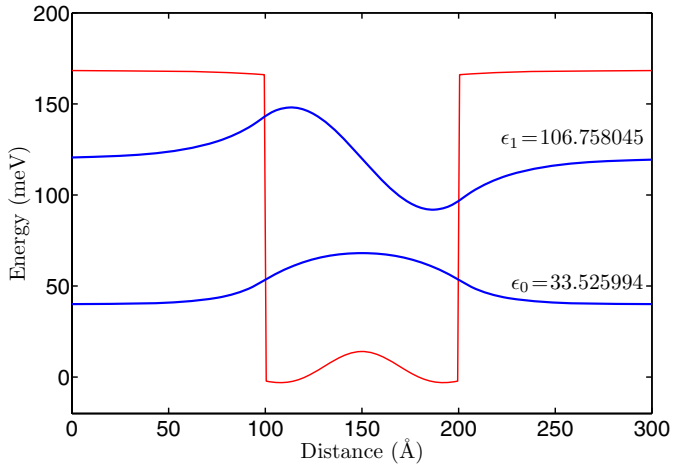


**Figure 4.** Eigenstates of the in-well doped single well described in the text.

again, the well to be 100 Å wide consisting of $Al_{0.33}Ga_{0.67}As$ surrounded by GaAs barriers. The shape of the well is described by the barrier $V_{\text{out}} = 166/E_0 \exp(-1/(16x)^2+1/64)$ and the inside well $V_{\text{in}} = 1/4 \sin(3.4\pi x)/(3.4\pi x)$. Figure 4 shows the eigenvalues and normalized eigenfunctions for the first two states.

To conclude this section we examine a truly arbitrary potential. As stated above, single parabolic potentials have been extensively analyzed and will not be considered here, since the only jump they exhibit is on the mass. Instead we construct a well by replacing half of a parabolic potential with an exponential potential [11], of the form $V(x) = V_0 \exp(-1/(16x)^2 + 1/64), 0 < x < 1/2$, making the total potential profile asymmetric. This potential may have minor physical importance but demonstrates the efficiency of our method. The results for this potential are shown in figure 5. If the total potential was simply the exponential there would exist only the ground state, however, the asymmetry, namely the addition of the parabolic potential allows for a second eigenstate.

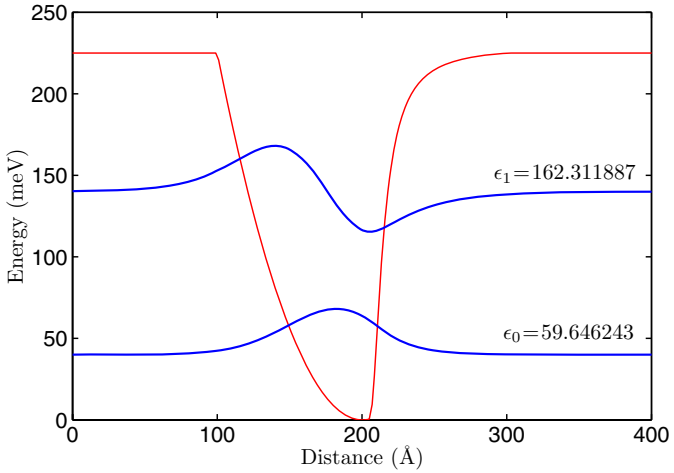


**Figure 5.** Eigenstates of an asymmetric parabolic-exponential potential.

Also, since the potential is narrowed in width due to the asymmetry there now exist only two eigenstates. Again these differences arise from the broken symmetry. The potential of figure 5 exhibits features from both parts of the (symmetric) potential (parabolic and super-potential) that it is constructed from, as expected.

## 4. Multiple potentials

Superlattice structures have been used in field effect transistors where several quantum wells provide parallel conducting channels, increasing the device current carrying capabilities and, hence, the output power. In heterostructure devices, superlattice buffers are used to create an intermediate layer between a substrate and an active layer. This allows us to alleviate strain caused by lattice constant mismatch and to obtain a much better quality active layer material. The addition of multiple potentials in equation (1) changes significantly its properties and dramatically increases the difficulty of finding an exact solution. Indeed, even for constant potentials the exact closed-form solution for the eigenvalue is an algebraic equation which has to be solve numerically. Hence, if the spectrum of single potentials for which the equation exhibits exact solutions is narrow the relative spectrum for multiple potentials is almost nonexisting making the use of numerical techniques a necessity.

To start our analysis and demonstrate the convergence and accuracy of the method we consider a series of truncated parabolic potentials, as in [11]. In figure 6 we plot the ground state and the first two excited states. In table 2 we show the convergence of the second (see appendix) and higher order methods.

One of the most interesting applications of superlattices is the quantum cascade laser [13]. Quantum cascade lasers (QCLs) are semiconductor lasers that emit in the mid- to far-infrared portion of the electromagnetic spectrum. Unlike typical interband semiconductor lasers that emit electromagnetic radiation through the recombination of electron-hole pairs across the material band gap, QCLs are unipolar and laser emission is achieved through the use of intersubband transitions in a repeated stack of semiconductor superlattices. To resemble such lattices we construct a potential after [14, 15]. The corresponding eigenstates are shown in figure 7.

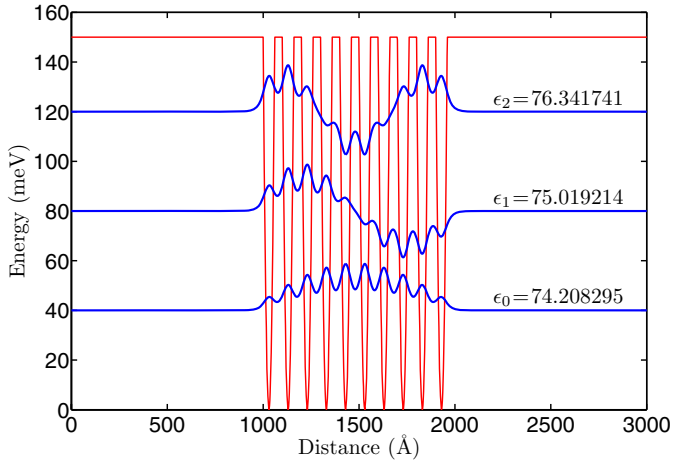


**Figure 6.** Eigenstates of a series of symmetric truncated parabolic potentials.

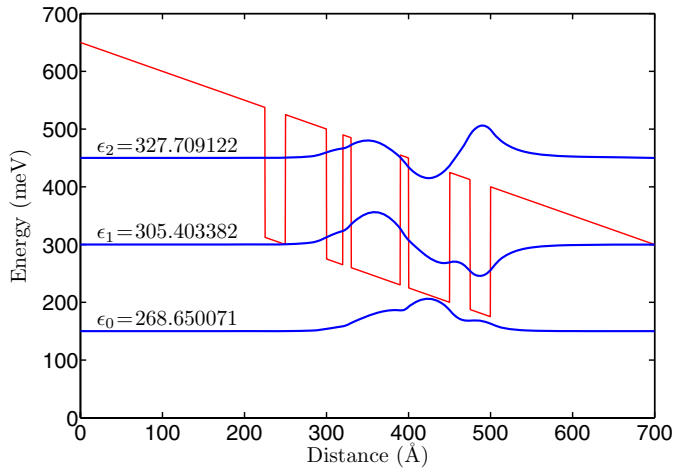


**Figure 7.** Eigenstates of the constructed superlattice in the text.

**Table 2.** The energy of a series of symmetric truncated parabolic potentials using second and fourth accurate methods.

| Number of points | Second-order results | Fourth-order results |
|---|---|---|
| 500 | 75.099 306 76 | 74.853 667 09 |
| 1 000 | 74.435 367 96 | 74.263 543 84 |
| 2 000 | 74.265 161 91 | 74.212 237 67 |
| 4 000 | 74.222 525 30 | 74.208 558 41 |
| 8 000 | 74.211 895 17 | 74.208 312 09 |
| 16 000 | 74.209 189 15 | 74.208 296 27 |
| 32 000 | 74.208 518 20 | 74.208 295 27 |
| 64 000 | 74.208 351 56 | 74.208 295 27 |

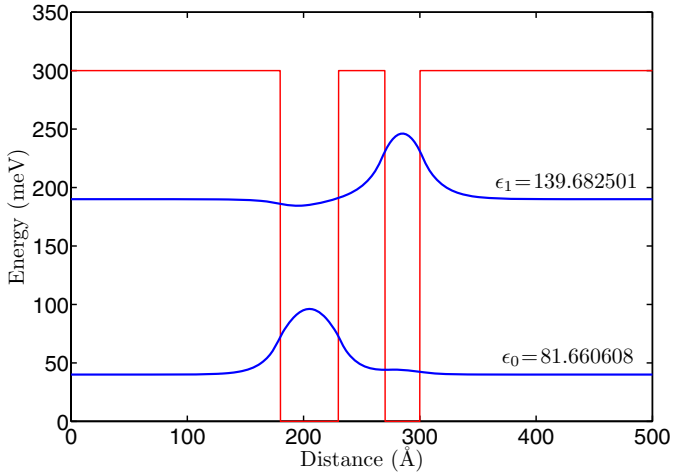


**Figure 8.** Eigenstates of an asymmetric potential.

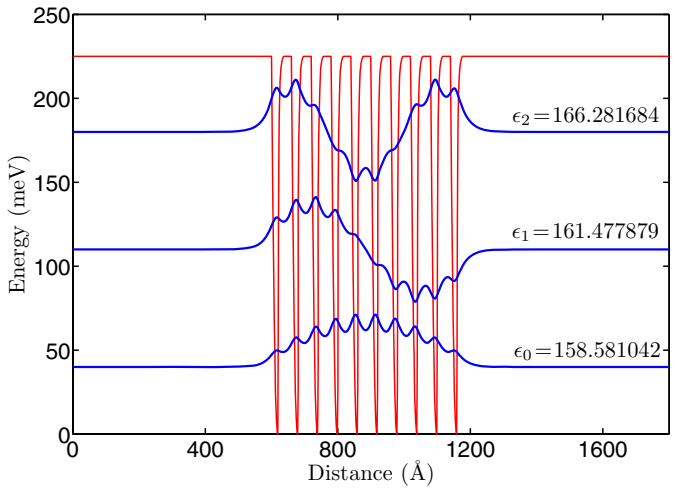


**Figure 9.** Eigenstates of a general multi-well potential.

Laser diodes and amplifiers based on asymmetric quantum-well heterostructures are also of importance [16]. In contrast to ordinary laser heterostructures, for such modified quantum-well systems, it is possible to change the gain spectrum in a wide range and to control the set of definite amplification frequencies by selecting the width and component composition of quantum wells and barrier regions. For the asymmetric potential of [16], namely width of 50-40-30 (well, barrier, well) in Å, the only existing states are shown in figure 8. As expected the break in the symmetry of the potentials results in the lift of any degeneracy in the eigenstates.

Finally, like in the case of a single potential we consider a series of arbitrary potentials. The left-half of each potential is parabolic while the right-half part is the super-exponential of the previous section, the results are depicted in figure 9. Each single potential is the same as

that of the previous section; spacing between wells is 24 Å and their width is 36 Å. Note that the addition of multiple wells now allows for higher states to exist.

## 5. Conclusions

In recent years there has been a considerable increase in research activities directed toward the development of optoelectronic devices based on quantum-well structures. The work and time spent to develop a new device is, however, very high and in order to better understand the physical properties of a device it is important that one can simulate the expected performance numerically. The proposed technique must be such that scientists working with it, without expert knowledge in numerical computation, must be able to implement computer models, appropriate to their problem, on their own. Furthermore, they must be tested on a wide range of structures to ensure that they are well behaved.

To meet this need we have introduced a simple numerical technique based on finite differences to calculate the eigenstates of arbitrary quantum structures. This is a direct generalization of the method presented in [11] to higher-order. The main advantages are that it requires no alternation for different types of potentials—the potential needs not be symmetric, it can be discontinuous and even singular in terms of delta functions—, it can be extended to higher order and even to handle two-dimensional problems and can be used for a wide area of problems originating from quantum-well structures to quantum dots and wires. Even higher orders (sixth, etc) can be achieved following the above procedure. However, that should be done with care since the more accurate the method the more points need to be replaced thus increasing the total number of points in the grid.

## Acknowledgments

D J Costinett acknowledges financial support from the Department of Applied Mathematics, University of Colorado, under grant NSF-MCTP-0602284.

## Appendix A. The second order method

The basic steps of the method remain the same for any order. Specifically, for second order accuracy we wish to approximate equation (1) with a differencing scheme of the form

$$\sigma_1\psi_{i-1} + \sigma_2\psi_i + \sigma_3\psi_{i+1} = \epsilon\psi_i$$

where now we only need to replace the coefficients for two irregular points, as shown in figure A1. For all other points

$$\sigma_1 = \sigma_3 = -\frac{M(x_i)}{h^2}, \qquad \sigma_2 = \frac{2M(x_i)}{h^2} + V(x_i).$$

The only jump conditions needed are for the function and its first two derivatives (same as in the text). The major difference from the higher-order method is the expansion in the functions, namely the nominal Taylor expansion would be

$$\psi_i = \psi + (x_i - x^*)\psi_x + \tfrac{1}{2}(x_i - x^*)\psi_{xx} + O(h^3),$$

and the right-hand side of the equation needs no further expansion, i.e. $\epsilon\psi_i = -M(x_i)\psi_{xx} + V(x_i)\psi_i$. The resulting systems are then, at $x_j$

$$\sigma_1 + \sigma_2 + \sigma_3\left[1 + \frac{1}{2}(x_{j+1} - x^*)^2\frac{V^+ - V^-}{M^+}\right] = V^- \tag{A.1}$$

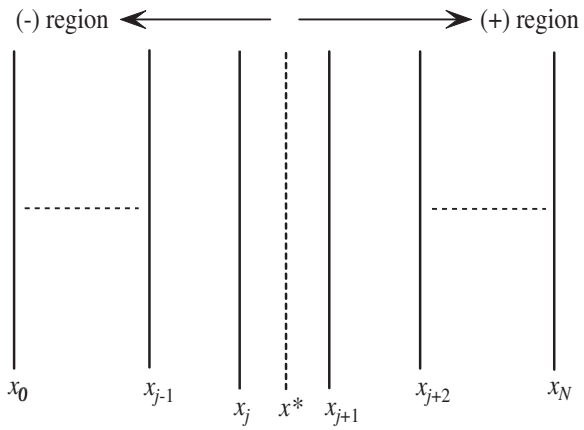


**Figure A1.** The uniform grid, the irregular points and the interface of the second order method.

$$\sigma_1(x_{j-1}-x^*)+\sigma_2(x_j-x^*)+\sigma_3(x_{j+1}-x^*)\frac{M^-}{M^+}=0 \tag{A.2}$$

$$\sigma_1\frac{1}{2}(x_{j-1}-x^*)+\sigma_2\frac{1}{2}(x_j-x^*)+\sigma_3\frac{1}{2}(x_{j+1}-x^*)\frac{M^-}{M^+}=-M^- \tag{A.3}$$

and at $x_{j+1}$

$$\sigma_1\left[1+\frac{1}{2}(x_j-x^*)^2\frac{V^--V^+}{M^-}\right]+\sigma_2+\sigma_3=V^+ \tag{A.4}$$

$$\sigma_1(x_{j-1}-x^*)\frac{M^+}{M^-}+\sigma_2(x_j-x^*)+\sigma_3(x_{j+1}-x^*)=0 \tag{A.5}$$

$$\sigma_1\frac{1}{2}(x_{j-1}-x^*)\frac{M^+}{M^-}+\sigma_2\frac{1}{2}(x_j-x^*)+\sigma_3\frac{1}{2}(x_{j+1}-x^*)=-M^+. \tag{A.6}$$

For more details see [11].

## Appendix B. Boundary conditions for higher order differences

As usual, special care must be given to the end points. High-order methods require an extrapolation scheme to determine the differencing coefficients at $x_2$ and $x_{N-1}$. Given the boundary conditions $\psi(x_0)=\psi_1=0$ and $\psi(x_N)=\psi_N=0$ and using the extrapolation

$$\psi_0=-\psi_4+4\psi_3-6\psi_2+4\psi_1$$
$$\psi_N=-\psi_{N-1}+4\psi_{N-2}-6\psi_{N-3}+4\psi_{N-4}$$

we have

$$\left(\frac{2M}{h^2}+V\right)\psi_2+\left(\frac{-M}{h^2}\right)\psi_3+(0)\,\psi_4=\epsilon\psi_2$$
$$\left(\frac{2M}{h^2}+V\right)\psi_{N-2}+\left(\frac{-M}{h^2}\right)\psi_{N-3}+(0)\,\psi_{N-4}=\epsilon\psi_{N-2}$$

for $i=2$ and $N-1$, respectively.

## References


[1] Ando T and Mori S 1982 Effective-mass theory of semiconductor heterojunctions and superlattices *Surf. Sci.* **113** 124

[2] Nakamura K, Shimizu A, Koshiba M and Hayata K 1989 Finite-element calculation of the transmission probability and the resonant-tunneling lifetime through arbitrary potential barriers *IEEE J. Quantum. Electron.* **25** 1189

[3] Le K Q 2009 Finite element analysis of quantume states in layered quantum semiconductor structures with band nonparabolicity effect *Microw. Opt. Technol. Lett.* **51** 1

[4] Jonsson B and Eng S 1990 Solving the Schrödinger equation in arbitrary quantum-well potential profiles using the transfer matrix method *IEEE J. Quantum. Electron.* **26** 2025

[5] Zhang A, Cao Z, Shen Q, Dou X and Chen Y 2000 Tunnelling coefficients across an arbitrary potential barrier *J. Phys. A: Math. Gen.* **33** 5449

[6] Ando T, Taniyama H, Ohtani N, Hosoda M and Nakayama M 2002 Numerically stable and flexible method for solutions of the Schrödinger equation with self-interaction of carriers in quantum wells *IEEE J. Quantum. Electron.* **38** 1372

[7] Harrison P 2005 *Quantum Wells, Wires and Dots* (New York: Wiley-Interscience)

[8] Davé D 1991 Numerical technique to calculate eigenenergies and eigenstates of quantum wells with arbitrary potential profile *Electron. Lett.* **27** 1735

[9] Liu Q, Cheng C and Massoud H 2004 The spectral grid method: A novel fast Schrödinger-equation solver for semiconductor nanodevice simulation *IEEE. T. Comput. Aid. D.* **23** 1200

[10] Rieth M, Schommers W and Baskoutas S 2002 Exact numerical solution of Schrödinger's equation for a particle in an interaction potential of general shape *Int. J. Mod. Phys.* B **16** 4081

[11] Horikis T 2006 Eigenstate calculation of arbitrary quantum structures *Phys. Lett.* A **359** 345

[12] Leveque R and Li Z 1994 The immersed interface method for elliptic equations with discontinuous coefficients and singular sources *SIAM J. Numer. Anal.* **31** 1019

[13] Faist J, Capasso F, Sivco D, Sirtori C, Hutchinson A and Cho A 1994 Quantum cascade laser *Science* **264** 554

[14] Kruck P, Page H, Sirtori C, Barbieri S, Stellmacher M and Nagle J 2000 Improved temperature performance of $Al_{0.33}Ga_{0.67}As/GaAs$ quantum-cascade lasers with emission wavelength at $\lambda \approx 11$ $\mu$m *Appl. Phys. Lett.* **76** 3340

[15] Becker C, Sirtori C, Page H, Glastre G, Ortiz V, Marcadet X, Stellmacher M and Nagle J 2000 AlAs/GaAs quantum cascade lasers based on large direct conduction band discontinuity *Appl. Phys. Lett.* **77** 463

[16] Juang C, Kuhn K and Darling R 1991 Electric field effects in AlGaAs-GaAs symmetric and asymmetric coupled quantum wells *IEEE J. Quantum. Electron.* **27** 2122